Earth and Planetary Science Letters 536 (2020) 116138

Contents lists available at ScienceDirect

Earth and Planetary Science Letters

www.elsevier.com/locate/epsl

Formation of lunar highlands anorthosites

Xiaoqing Xu [a], Hejiu Hui [a,b,*], Wei Chen [c], Shichun Huang [d], Clive R. Neal [e], Xisheng Xu [a]

[a] State Key Laboratory of Mineral Deposits Research & Lunar and Planetary Science Institute, School of Earth Sciences and Engineering, Nanjing University, Nanjing 210023, China
[b] CAS Center for Excellence in Comparative Planetology, Hefei 230026, China
[c] State Key Laboratory of Geological Processes and Mineral Resources, School of Earth Sciences, China University of Geosciences, Wuhan 430074, China
[d] Department of Geoscience, University of Nevada, Las Vegas, NV 89154, United States
[e] Department of Civil and Environmental Engineering and Earth Sciences, University of Notre Dame, Notre Dame, IN 46556, United States

ARTICLE INFO

Article history:
Received 17 July 2019
Received in revised form 3 January 2020
Accepted 4 February 2020
Available online xxxx
Editor: F. Moynier

Keywords:
lunar magma ocean
lunar crust
lunar anorthosite
lunar mantle
KREEP
metasomatism

ABSTRACT

The lunar magma ocean (LMO) model was proposed after the discovery of anorthosite in Apollo 11 samples. However, the chemical and isotopic compositions of lunar anorthosites are not fully consistent with its LMO origin. We have analyzed major and trace elements in anorthositic clasts from ten lunar feldspathic meteorites, which are related to the solidification of the LMO. The plagioclase rare earth element (REE) abundances and patterns are not correlated with the Mg# of coexisting mafic minerals in anorthosites, implying that mafic minerals and plagioclase may not be in chemical equilibrium, consistent with their textural differences. The REE abundances in plagioclase range approximately fortyfold, which cannot be produced by fractional crystallization of a single magma. Combining plagioclase trace element data from Apollo and meteoritic anorthosites, we propose that plagioclases derived from the LMO floated to the surface to form the primordial crust, which then may have been metasomatized by incompatible-element-rich KREEP (potassium, rare earth element, phosphorus) melts and mantle-derived partial melts. The lunar anorthosites may represent this metasomatized crust rather than solely a derivative from the LMO. Furthermore, silicate melts similar to the metasomatic agents may also have melted the crust to form the Mg-suite rocks. This hypothesis is consistent with overlapping ranges of age and initial ε_{Nd} between lunar anorthosites and Mg-suite rocks. These events are consistent with an overturn event of the cumulate mantle very early after primordial crust formation to produce the partial melts that metasomatized the crust.

1. Introduction

The Moon's energetic formation process (e.g., Canup and Asphaug, 2001) has been proposed to result in a lunar magma ocean (LMO) (Warren, 1985; Shearer et al., 2006). The primordial feldspathic crust has been proposed to form from floating plagioclase that crystallized from the LMO, whereas the mare basalts and picritic glasses were partial melts of LMO cumulates consisting of denser mafic minerals (Warren, 1985; Snyder et al., 1992; Hess and Parmentier, 1995; Elardo et al., 2011; Elkins-Tanton et al., 2011). The LMO model is consistent with the prevailing negative Eu anomalies observed in mare basalts and picritic glasses (suggesting the source regions had experienced plagioclase removal), the global occurrence of plagioclase on the lunar surface (Shearer et al., 2006), and the general uniformity of the incompatible trace element (ITE) patterns among KREEP (potassium, rare earth element, phosphorus) rocks (Warren, 1989). The LMO model is a fundamental hypothesis for understanding the evolution of the Moon, and the magma ocean model has also been applied to other silicate planetary bodies (e.g., Elkins-Tanton, 2012). However, recent findings from lunar samples and remote sensing data have challenged the classical LMO model (e.g., Borg et al., 2011; Ohtake et al., 2012; Gross et al., 2014).

The recalculated ^{147}Sm-^{143}Nd ages of ferroan anorthosite (FAN) collected during the Apollo program span a wide range, from 4.29 Ga to 4.57 Ga, overlapping with that (4.16–4.57 Ga) of highlands Mg-suite (HMS) samples (Borg et al., 2015). By contrast,

* Corresponding author at: State Key Laboratory of Mineral Deposits Research & Lunar and Planetary Science Institute, School of Earth Sciences and Engineering, Nanjing University, Nanjing 210023, China.
E-mail address: hhui@nju.edu.cn (H. Hui).

https://doi.org/10.1016/j.epsl.2020.116138
0012-821X/

the LMO model predicts that the feldspathic crust would have formed during LMO solidification and before the formation of Mg-suite plutons, which have been suggested to be the product of interactions between anorthositic crust and the mantle-derived melts (Warren, 1985; Shearer et al., 2015). Borg et al. (2019) concluded that the derivation of mare basalt sources and some FANs from a common reservoir formed at 4.34 Ga was not consistent with an early solidification of the LMO. Furthermore, the recalculated initial ε_{Nd} values of lunar anorthosite range from positive to negative ($+3.49\pm0.98 \sim -0.24\pm0.09$; Borg et al., 2015). This large variation indicates that the magma sources of lunar anorthosites range from light REE (LREE)-depleted to LREE-enriched, which is inconsistent with the classical LMO model (e.g., Snyder et al., 1992). Plagioclase in Apollo FANs is highly calcic with An [molar Ca/(Ca+Na+K)×100] > 94, whereas the coexisting mafic minerals pyroxene and olivine are relatively Fe-rich with Mg# [molar Mg/(Mg+Fe)×100, all Fe as Fe^{2+}] mostly ranging from ~40 to ~70 (e.g., McGee, 1993; Warren, 1993). By contrast, although anorthosites from lunar meteorites have similar An-rich plagioclase, they contain mafic minerals with Mg# as high as 90, which could not have been derived by crystal fractionation of a LMO (Takeda et al., 2006; Mercer et al., 2013; Gross et al., 2014). Finally, complex trace element variations in plagioclase from Apollo and meteoritic anorthosites are not consistent with those in anorthositic plagioclase derived from a single magma reservoir (Palme et al., 1984; Floss et al., 1998; Russell et al., 2014).

The serial magmatism model has been proposed as an alternative to the classical LMO model for interpreting the occurrence of anorthosite on the Moon (Jolliff and Haskin, 1995; Longhi, 2003; Gross et al., 2014). This formation scenario for lunar anorthosites can yield a complex crust over a long period of time, which may explain the broad age range and large compositional variations observed in lunar anorthosites (Gross et al., 2014; Borg et al., 2015; Shearer et al., 2015). However, crystallization of basaltic intrusions may not yield Fe-rich mafic minerals with highly An-rich plagioclase in lunar anorthosites unless the alkali contents of the melt are nearly zero (Namur et al., 2011). Furthermore, this model cannot explain the observation that lunar anorthosites have relatively uniform An-rich plagioclases (An > 94) that are not texturally or compositionally in equilibrium with coexisting mafic minerals (Namur et al., 2011; Nekvasil et al., 2015). Indeed, the high-Al basalts derived from partial melting of the lunar mantle could have contained plagioclase with An varying from 73 to 96 (Hui et al., 2011). More significantly, serial magmatism could not produce the uniformity of the ITE patterns among KREEP rocks (e.g., Warren, 1985; 1989).

The formation of lunar anorthosite remains an unresolved issue. The Apollo sampling sites were limited in area within or close to the Procellarum KREEP Terrane on the near side of the Moon, which suggests that the Apollo samples may not be sufficiently representative to elucidate the global evolution of the Moon, including the LMO. However, meteorites randomly ejected from unknown locations on the Moon may be more representative than, or at least complementary to, the Apollo samples (Korotev, 2005). In this study, we selected a suite of lunar feldspathic breccia meteorites and performed detailed *in situ* geochemical analyses on their anorthositic clasts. Combined with literature data for Apollo and meteoritic anorthosites, our results shed light on the formation of lunar anorthosite and on the evolution of the LMO.

2. Samples and analytical methods

2.1. Scanning electron microscope (SEM)

Ten lunar meteorites were selected for our geochemical analyses. These meteorites are feldspathic breccia, including NWA 5406, NWA 6721, NWA 7493, NWA 8181, NWA 8609, NWA 10228, NWA 10415, Dho 1669, Dho 1769, and Dho 1528. The meteorite chips were embedded in epoxy resin and polished into thick sections. The sections were cleaned with MQ H_2O and then dried at room temperature. They were stored in a desiccator until petrographic and chemical analyses were performed. Backscattered electron (BSE) images of carbon-coated sections were obtained using a JEOL JSM-6490 scanning electron microscope at the State Key Laboratory of Mineral Deposits Research, Nanjing University. An electron beam with 15 kV accelerating voltage was used. Anorthositic clasts were identified in ten thick sections for major and trace element analyses using the mosaicked BSE images.

2.2. Electron probe microanalyzer (EMPA)

Major element compositions of plagioclase, olivine, and pyroxene in selected clasts from our lunar meteorites were analyzed using a JEOL JXA-8230 electron probe microanalyzer at the Testing Center of the China Metallurgical Geology Bureau, Shandong Branch. Point analyses were performed on all the mineral grains using an electron beam with 15 kV accelerating voltage. Plagioclase was analyzed using a 5 μm diameter electron beam with 10 nA current. Olivine and pyroxene were analyzed using a 1 μm diameter electron beam with 20 nA current. Both natural and synthetic crystals were used as standards for the analyses. ZAF correction was applied to all analyses.

2.3. LA-ICP-MS

Trace element compositions of plagioclase were analyzed using a Thermo Scientific iCAP Q inductively coupled plasma mass spectrometry coupled to a 193 nm RESOlution-S155 ArF excimer laser ablation system (LA-ICP-MS) at the State Key Laboratory of Geological Processes and Mineral Resources, China University of Geosciences (Wuhan). Standards and samples were analyzed using a laser beam with 50 μm diameter, 10 Hz repetition rate, and ~3 J/cm^2 energy output density. Each analysis consisted of ~30 s background collection (gas blank) and ~40 s laser ablation of the sample. Calcium was used as an internal standard for calibration using the concentration determined by EMPA. USGS reference glasses (BCR-2G, BIR-1G, and BHVO-2G) and NIST glasses (SRM610 and SRM614) were analyzed as external standards. NIST SRM 612 glass was used to correct the instrument drift. These bracketing standards were analyzed every 5 to 6 sample analyses. In addition, MPI-DING glasses (GOR-128-G and GOR-132-G), which have REE contents similar to those of our lunar plagioclase, were measured as unknowns to assess the accuracy and reproducibility of plagioclase trace element determinations. Raw count rate data, including concentration, detection limit, and uncertainty, were reduced using the ICPMSDataCal software (Liu et al., 2008). The analytical uncertainties for most trace elements are within 10% based on repeated measurements of MPI DING glasses (Table S3).

3. Results

Fifty-one anorthositic clasts from ten lunar feldspathic meteorites were analyzed in this study (Table 1; Figs. 1 and S1). The clast sizes range from 0.3 mm to 1.6 mm in length, and most are larger than 0.5 mm (Table 1). The anorthositic clasts are primarily composed of plagioclase (>96%), and 25 clasts contain trace amounts of mafic mineral (olivine, pigeonite, augite, and/or ilmenite) (Table 1; Figs. 1 and S1). The mafic minerals exhibit fine-grained xenomorphic granular texture. All plagioclases have been shocked, and some may even have been partially converted to maskelynite (Figs. 1 and S1).

Table 1
Summary of the lunar meteorites analyzed in the present study.

Sample	Clast type	Anorthositic clasts				
		An	Pgt Mg#	Aug Mg#	Ol Mg#	Clast size (mm)
NWA 5406	anorthosite, granulite	96.0–97.9		72.2–72.7		0.6–1.1
NWA 6721	anorthosite, basalt, granulite, impact melt	96.3–97.2		57.9	74.2–74.8	0.4–0.6
NWA 7493	anorthosite, basalt, granulite, impact melt	96.8–97.7	66.4–73.1	73.4	68.5–74.2	0.3–0.8
NWA 8181	anorthosite	95.9–97.2			66.0–74.8	0.3–1.0
NWA 8609	anorthosite, granulite, impact melt	95.2–97.2				0.3–1.3
NWA 10228	anorthosite, impact melt	95.5–97.3			71.0–74.8	0.3–0.9
NWA 10415	anorthosite, granulite, impact melt	95.4–98.5	59.1–66.2		60.4–80.1	0.5–1.6
Dho 1669	anorthosite, impact melt	98.2–98.5				0.5
Dho 1769	anorthosite, basalt, granulite, impact melt	95.5–97.6	49.9–66.0		62	0.7–0.8
Dho 1528	anorthosite, basalt, granulite, impact melt	95.7–97.5		59.8–65		0.4–0.6

An, anorthite; Pgt, pigeonite; Aug, augite; Ol, olivine.

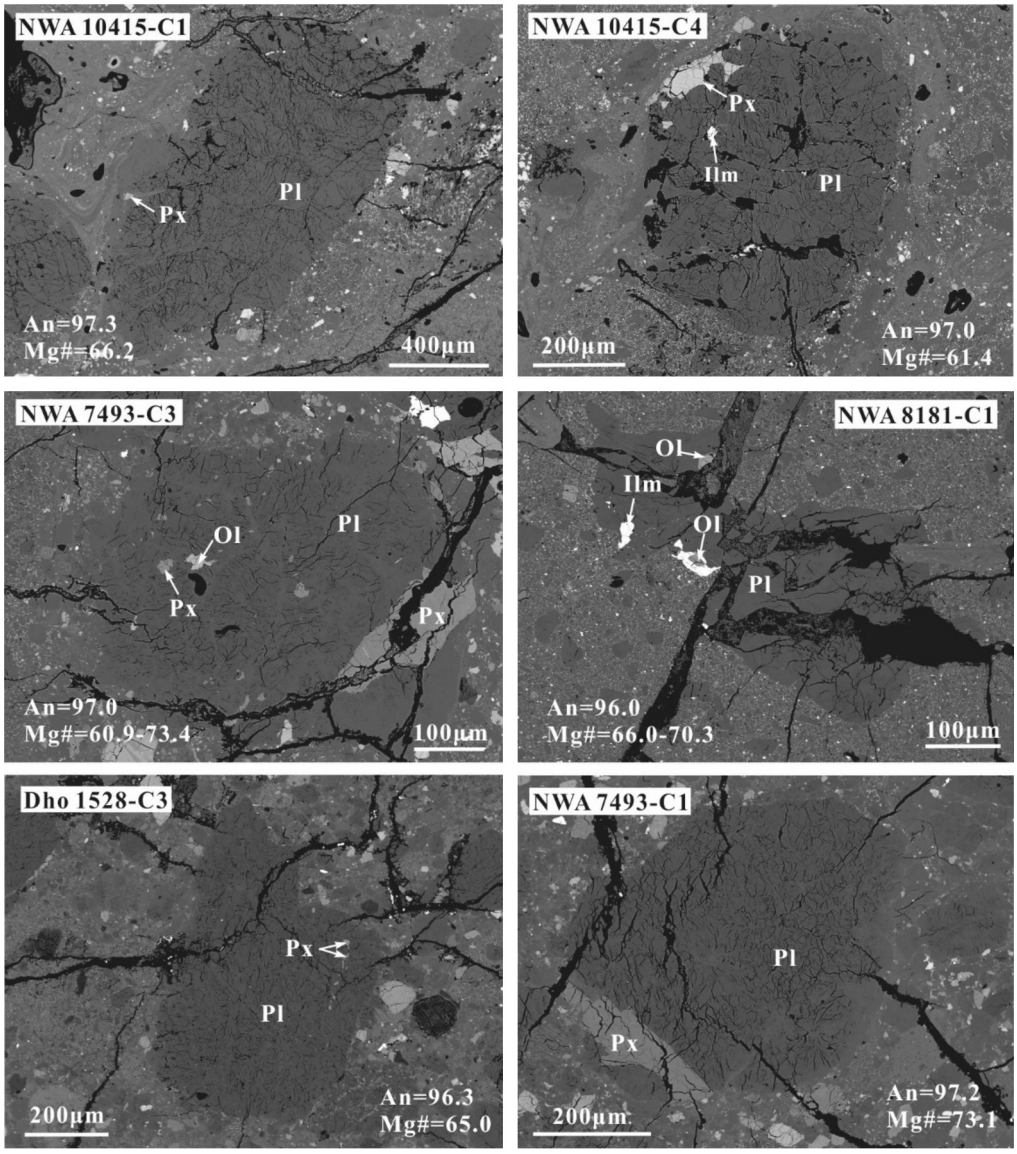

Fig. 1. Back-scattered electron (BSE) images of typical anorthositic clasts analyzed in the present study. Pl, plagioclase; Px, pyroxene; Ilm, Ilmenite.

3.1. Major elements

The anorthite contents of plagioclase are homogeneous within each clast at ±0.5% level, but vary from 95.3 to 98.4 among the different clasts from this suite of meteorites (Fig. 2; Table S1), similar to reported values for Apollo anorthosites (Papike et al., 1997; Floss et al., 1998) and meteoritic anorthositic clasts (Gross et al., 2014; Russell et al., 2014). The major element compositions of mafic minerals (olivine and pyroxene) vary slightly within each clast and significantly among different clasts (Figs. 1 and S1). Olivine Mg# ranges from 60.4 to 80.1, and pyroxene Mg# varies from 49.9 to 74.3 (Fig. 2a; Table S2). Some clasts with Mg-rich

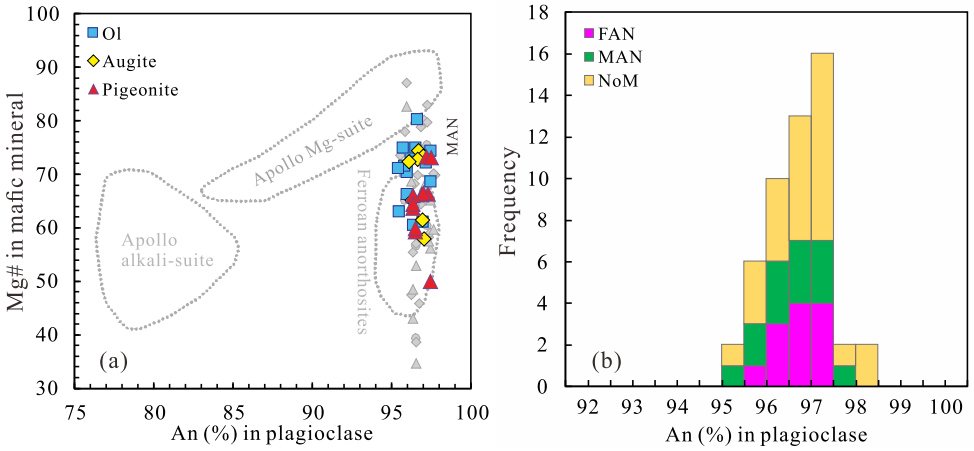

Fig. 2. Variations in anorthite content (An) in anorthositic clasts analyzed in the present study. (a) Mg# in mafic mineral versus anorthite content in coexisting plagioclase. Gray symbols represent anorthositic clasts in lunar meteorites ALHA 81005 and NWA 2996 (Gross et al., 2014). The compositional fields of Apollo ferroan anorthosites, magnesian-suite rocks, and alkali-suite rocks (Lindstrom et al., 1989) are shown for comparison. (b) Histogram of anorthite content of plagioclase in anorthositic clasts analyzed in the present study.

mafic minerals are magnesian anorthosites (MAN) that fall in the gap between FAN and HMS (Fig. 2a). The MAN clasts differ from the FANs in the Apollo collections (Lindstrom et al., 1989; McGee, 1993), but are similar to the MANs in other lunar meteorites (Takeda et al., 2006; Gross et al., 2014). Overall, the anorthositic clasts in our lunar meteorites (Fig. 2) are petrographically similar to previously described Apollo and meteoritic anorthosites (e.g., McGee, 1993; Gross et al., 2014). Based on the occurrence of mafic minerals, the anorthositic clasts analyzed in the present study can be divided into three groups: FAN clasts, MAN clasts, and anorthositic clasts without mafic minerals (NoM), which can be either FAN or MAN (Fig. 2b).

3.2. Trace elements

The plagioclase trace element concentrations within each clast are relatively homogeneous, but they vary significantly among different clasts (Fig. 3; Table S3). The plagioclase trace element abundances of different groups overlap with each other (Fig. 3; Table S3).

Plagioclase REE patterns in all anorthositic clasts show positive Eu anomalies, as do those in Apollo FANs (Fig. 3). The LREE abundances in plagioclase in FAN clasts are between 0.4 and 17.8 × abundances of CI chondrite (hereafter, × CI; Anders and Grevesse, 1989). Europium abundances vary from 12.7 to 27.9 × CI, and there are positive Eu anomalies in all measured plagioclases, with Eu/Sm ranging from 3.5 to 37.2 × CI (Fig. 3a). Heavy REE (HREE) abundances range from 0.07 to 3.2 × CI, and some are below our detection limits. The plagioclase REE patterns in MANs and NoMs are very similar to those in FANs (Fig. 3a–c; Table S3). Within each group, there is large variation in their plagioclase REE patterns. The plagioclase in FAN clast Dho 1769-C4 has a much lower and flatter REE pattern relative to that in another FAN clast Dho 1769-C11 (Fig. 3d). Similar differences have also been observed in MANs, such as clasts NWA 5406-C1 and NWA 10228-C6, and in NoMs, such as clasts NWA 6721-C5 and NWA 8609-C1 (Fig. 3d).

Zirconium abundances in plagioclase range from 0.05 to 10.6 ppm, and most are lower than 2 ppm, similar to those (0.07–14.8 ppm) reported for lunar meteoritic plagioclase (Cahill et al., 2004; Russell et al., 2014). Potassium abundances in our plagioclase vary from 18 to 1491 ppm, which are more variable than those (17–274 ppm) in Apollo anorthosites (Steele et al., 1980; Floss et al., 1998; Togashi et al., 2017), but overlap with those (249–3096 ppm) in plagioclase in Apollo Mg-suite rocks (Papike et al., 1996; Shervais and McGee, 1998). The ^{39}K signal was constant during each LA-ICP-MS analysis, similar to immobile elements, indicating that the higher K contents are not related to terrestrial contamination. Plagioclase Sr abundances vary from 155 to 500 ppm, and Ba abundances range from 2.3 to 138 ppm, similar to those reported for lunar meteoritic anorthosites (Sr: 144–531 ppm; Ba: 6.2–237 ppm; Russell et al., 2014; Pernet-Fisher et al., 2017) and Apollo anorthosites (Sr: 103–340 ppm; Ba: 3.1–225 ppm; Steele et al., 1980; Papike et al., 1997; Floss et al., 1998; Togashi et al., 2017). Low abundances of Sr and Ba in plagioclases are consistent with a low level of terrestrial contamination/alteration of meteorites (Russell et al., 2014).

4. Discussion

4.1. Inter-phase disequilibrium in lunar anorthosite

The mafic minerals in our monomict coarse-grained anorthositic clasts are small (typically less than 20 μm in length), rounded to subangular (Figs. 1 and S1), similar to those in lunar meteoritic anorthositic clasts (Gross et al., 2014). Furthermore, mafic minerals in Apollo anorthosites often exhibit poikilitic textures (James et al., 1989), which are considered to be evidence of crystallization from the interstitial liquid in the pore space (Namur et al., 2011). Therefore, at least some mafic minerals in lunar anorthosites may have formed after the crystallization of plagioclase. This possibility is consistent with the wide range of equilibrium temperatures (500–1200 °C) determined for mafic minerals in lunar anorthosites (Dixon and Papike, 1975; Evans et al., 1978; James et al., 2002).

Mafic minerals in lunar anorthositic clasts exhibit a large compositional range (Mg# = 50–80; Fig. 2a), consistent with previous observations (Mg# = 39–87) in meteorites ALHA 81005 and NWA 2996 (Gross et al., 2014). This compositional range is also similar to that (Mg# = 44–74) of the pristine (pristinity index > 7; An = 96 ± 1) Apollo anorthosites (Warren, 1993). The large variation cannot be derived from a fractional crystallization of a single magma reservoir even if it is coupled with adcumulate growth (Longhi, 1982; Gross et al., 2014). Crystallization of the interstitial liquid trapped in the matrix may produce the most Fe-rich mafic minerals (Mg# = 33–62) in anorthosites (Goodrich et al., 1984; Warren, 1993; Floss et al., 1998; Namur et al., 2011; Gross et al., 2014). However, this process cannot generate anorthosite containing mafic minerals with Mg# > 75 (Gross et al., 2014). On the other hand, calcic plagioclase without Na-enrichment could form at depths greater than ~70 km in the LMO during cooling

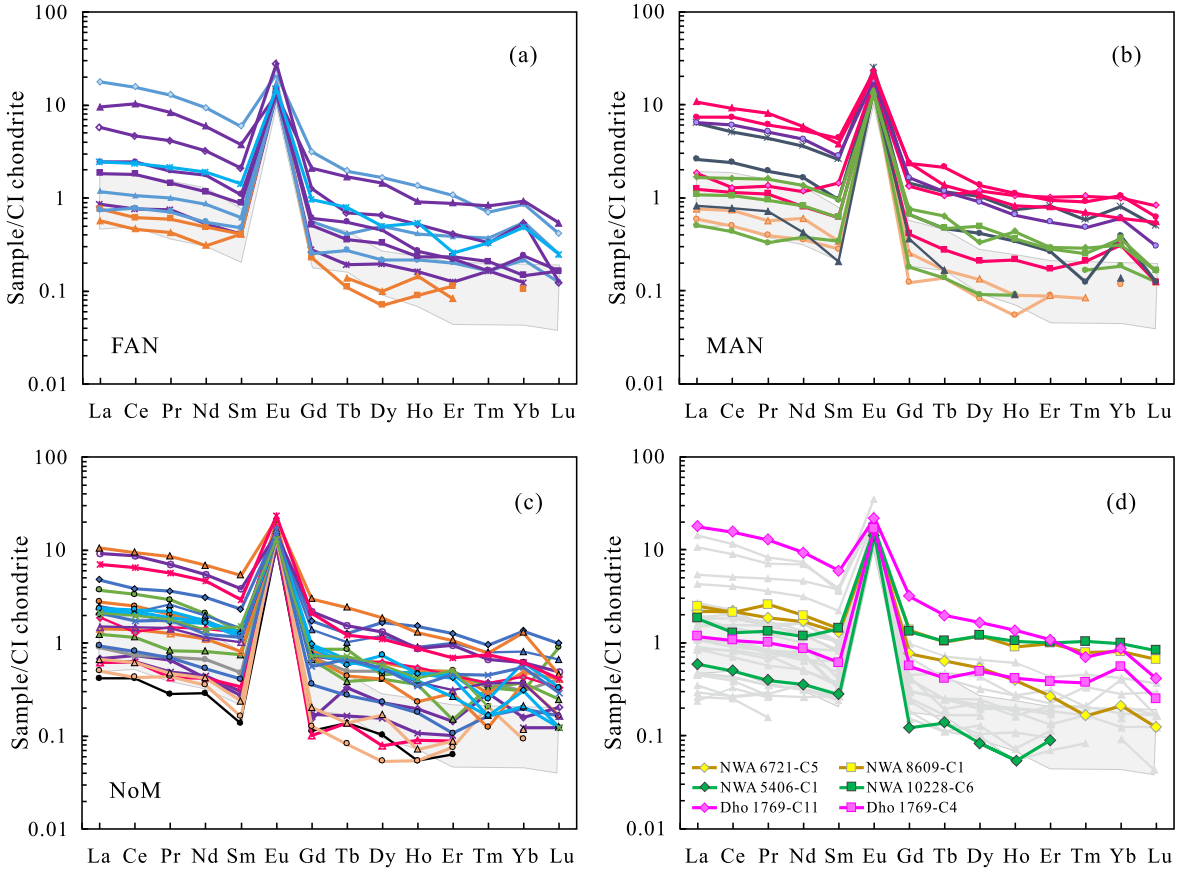

Fig. 3. CI-chondrite normalized rare earth element (REE) distribution patterns for plagioclase in anorthositic clasts analyzed in this study. (a) Plagioclase REE in ferroan anorthositic clasts (FAN), whose mafic minerals have Mg# $\leq$ 70. (b) Plagioclase REE in magnesian anorthositic clasts (MAN), whose mafic minerals have Mg# > 70. (c) Plagioclase REE in anorthositic clasts without mafic mineral (NoM). (d) Typical REE patterns in anorthositic plagioclase of different groups for comparison. CI chondrite values are from Anders and Grevesse (1989). Plagioclase REE range of Apollo FANs (Papike et al., 1997; Floss et al., 1998) is shown as shaded area for comparison. Plagioclase REE patterns for anorthositic clasts in lunar meteorites are represented by light gray lines. (Russell et al., 2014; Pernet-Fisher et al., 2017).

(Nekvasil et al., 2015), which may explain the absence of this correlation. However, this crystallization process cannot explain the plagioclase REE patterns in lunar anorthosites (see discussion below). Overall, the correlation between nearly constant An content of plagioclase and highly variable Mg# of mafic mineral (Fig. 2a) suggests that lunar anorthosites may be produced by complex processes beyond simple fractional crystallization in a single magma reservoir (e.g., James et al., 1989).

If both FANs and MANs formed from the same LMO, it is expected that MAN, which formed earlier than FAN, have lower REE abundances than FAN. However, there is no obvious REE difference between FAN and MAN clasts (Fig. 3a, b). Moreover, highly evolved plagioclase trace element compositions have been observed in some meteoritic anorthositic clasts containing mafic mineral with high Mg# (Fig. 3), which has also been observed in some Apollo MANs (e.g., Floss et al., 1998). This observation clearly is inconsistent with derivation of lunar anorthosites through fractional crystallization in a single evolving magma. Furthermore, the REE composition differences between plagioclases and their coexisting low-Ca pyroxenes in Apollo anorthosites cannot be explained using the experimentally determined partition coefficients (e.g., Floss et al., 1998), indicating that the coexisting minerals were not in equilibrium at magmatic conditions. Therefore, it appears that at least some lunar anorthosites have been affected by posy-crystallization processes (Dixon and Papike, 1975; Evans et al., 1978; James et al., 2002).

In summary, not all mafic minerals are in equilibrium with their coexisting plagioclases in lunar anorthosites. At least some mafic minerals resulted from interactions between the primordial anorthosite and infiltrating melts. The plagioclase grains, however, may have recorded both the primary and secondary processes.

4.2. Complex REE distributions in anorthositic plagioclase

The new plagioclase REE data acquired from three different groups of anorthositic clasts in this study cover the range reported for Apollo and meteoritic anorthosites (Fig. 4). The plagioclase REE patterns in different groups of anorthositic clasts are similar to those of Apollo anorthosites (Fig. 3a–c; Papike et al., 1997; Floss et al., 1998). However, plagioclases in some anorthositic clasts from lunar meteorites (e.g., clasts NWA 10228-C6 and Dho 1769-C4) have flatter REE patterns relative to those in Apollo FANs (Fig. 3d). This finding is consistent with the observation that anorthositic plagioclase in meteorite Dho 081 is less LREE-enriched relative to plagioclases in Apollo anorthosites (Russell et al., 2014).

It has been suggested that some lunar meteoritic plagioclases could have experienced REE evolution paths different from those in Apollo anorthosites, implying that lunar anorthosites could have multiple petrogeneses (Russell et al., 2014). Furthermore, the plagioclase REE variations in meteoritic anorthositic clasts, including the reported ranges (Russell et al., 2014; Pernet-Fisher et al., 2017), are much larger than those in Apollo FANs (Fig. 3). Plagioclase Nd concentrations in meteoritic anorthosites range from 0.13 to 4.20 ppm (Table S3), more variable than those in Apollo anorthositic plagioclases (0.14–1.99 ppm; Papike et al., 1997; Floss et al., 1998). Overall, the REE abundances in lunar anorthositic plagioclase vary by about fortyfold (Fig. 4; Table S3). However, the

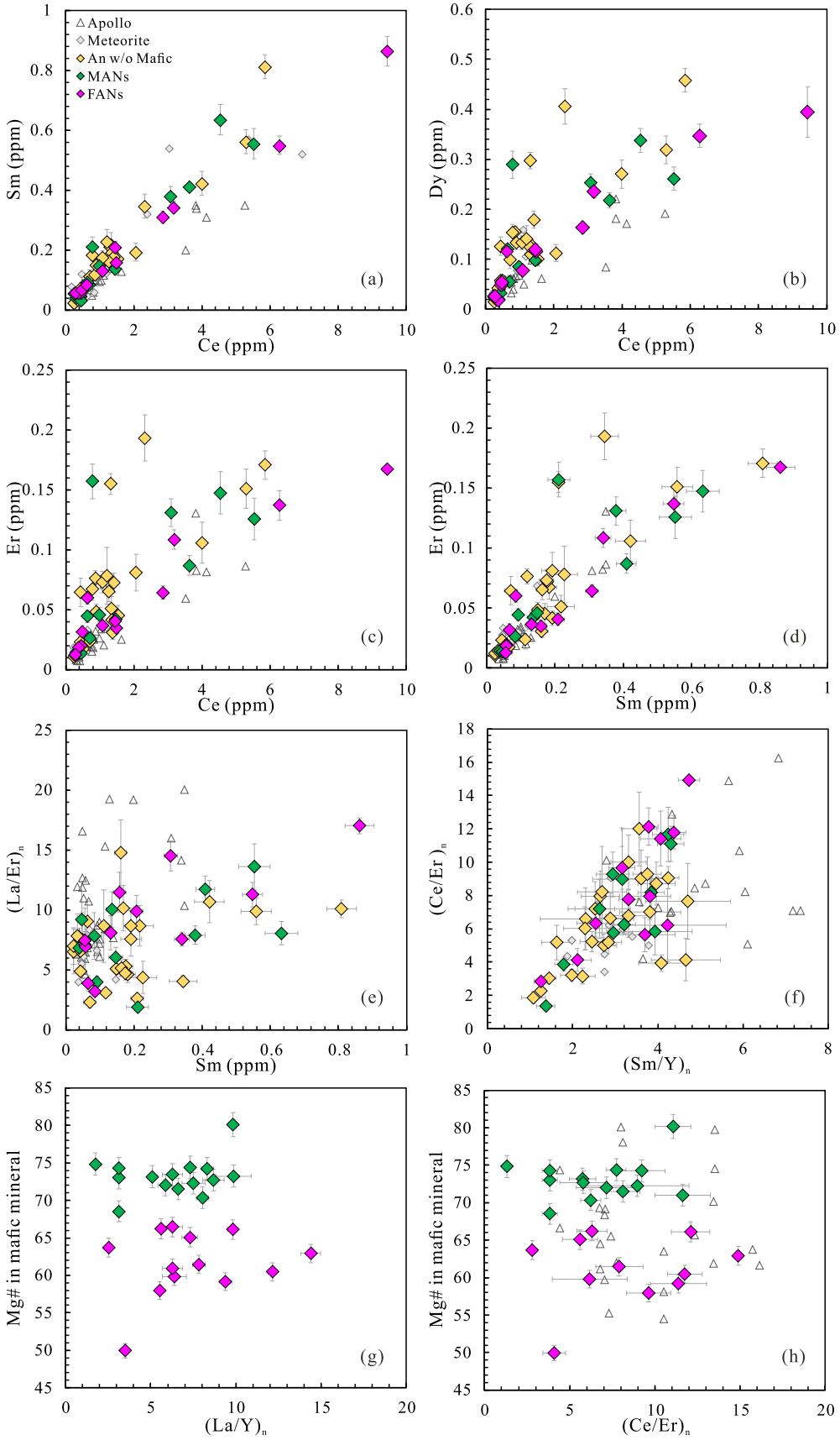

Fig. 4. Covariation of REE in plagioclase and Mg# in mafic mineral from the anorthositic clasts analyzed in this study. REE and Mg# data from Apollo anorthosites (Papike et al., 1997; Floss et al., 1998) and from previous studies of meteoritic anorthosites (Russell et al., 2014; Pernet-Fisher et al., 2017) are shown for comparison. Subscript "n" denotes chondrite normalized. The compositional data of lunar anorthosite are generally consistent with mixing of three end-members (see text for discussion).

Table 2
Trace element partition coefficients between plagioclase and melt.

Element	Rb	Sr	Y	La	Ce	Pr	Nd	Sm	Eu	Gd	Tb	Dy	Ho	Er	Tm	Yb	Lu
$K^{Pl/melt}$	0.0818	1.3	0.0025	0.0124	0.0116	0.0105	0.0092	0.0081	1.39	0.0046	0.0037	0.0029	0.0023	0.0019	0.0015	0.0013	0.0010

The partition coefficients were calculated for plagioclase $An_{97}Ab_3$ at $T = 1250\,^{\circ}C$ and $P = 0.46$ GPa (Sun et al., 2017). The major-element compositions used are average values of all anorthositic plagioclases analyzed herein.

Table 3
Trace element abundances in the three end-members.

Element	Rb	Sr	Y	La	Ce	Pr	Nd	Sm	Eu	Gd	Tb	Dy	Ho	Er	Tm	Yb	Lu
m-PAN	2.5	200	16	4.5	10.3	1.4	6.2	1.8	0.42	2.2	0.4	2.7	0.6	1.7	0.25	1.65	0.24
m-Mantle	2	150	645	20	61	11	70	29	0.7	60	12.4	93	24.2	78	12.8	91	14
m-KREEP	30	280	1000	590	1227	145	563	127	1.0	144	25.3	161	35.5	97	14.1	91	13

differences in REE abundance among plagioclases crystallized from the LMO have been suggested to be no more than fivefold when the LMO solidified from 78% to 95% (e.g., Snyder et al., 1992). This discrepancy suggests that lunar anorthositic plagioclases cannot be derived through simple fractional crystallization from a single magma.

4.3. Mixing of three end-members derived from the LMO

Rare earth element abundances and ratios typically evolve along almost linear trends as simple fractional crystallization of a single magma proceeds, which cannot result in the triangular compositional fields for anorthositic plagioclase (Fig. 4). In plots of REE versus REE, all three types of anorthosites overlap with each other (Fig. 4), indicating similar evolution history for both the FAN and the MAN. However, we note above that the REE abundance variations in anorthositic plagioclase (Figs. 3–4) are too large to be produced via simple fractional crystallization of the LMO (Snyder et al., 1992; Russell et al., 2014). The formation of the highlands anorthosites must involve melts from different source regions (Fig. 4).

Principal component analysis (PCA; Albarède, 1995) on chemical compositions of plagioclase from both Apollo and meteoritic anorthosites were used to assess the possible geochemical sources in anorthositic plagioclases. Eight REEs (La, Ce, Nd, Sm, Eu, Gd, Dy, Er) were used for the PCA. About 94% of the variance is explained by the first two independent principal components (Table S4; Fig. S3). That is, the lunar anorthosite plagioclase REE compositions define a 2-dimensional dataset. Consequently, at least three geochemical end-members are required to explain the lunar anorthositic plagioclase REE variations, consistent with the geochemical fields observed in REE plots (Fig. 4). The eigenvectors, or loadings, of each principal component (PC), do not define what three geochemical end-members are; however, they provide useful information to constrain the end-member compositions. PC1 has almost uniform loading from all REE, except for Eu (Table S4). This is consistent with the observation that most lunar anorthositic plagioclase REE patters are nearly parallel to each other (Fig. 3). That is, two geochemical end-members with subparallel REE patterns but different absolute REE abundances are responsible for PC1. The eigenvectors of PC2 decrease from LREE to HREE except for Eu. Thus, PC2 suggests that two geochemical end-members have opposite REE patterns (i.e., LREE-enriched and LREE-depleted). In the following, we will use this as a guide to understand the plagioclase REE compositions of lunar anorthosite.

We used the most recent partitioning model for trace elements between plagioclase and basaltic melt (Sun et al., 2017), which is based on the experiments with lunar relevant compositions and conditions, to calculate the REE compositions of melt in equilibrium with anorthositic plagioclases (Table 2). The REE patterns of all the equilibrium melts show negative Eu anomalies with very large variations in their abundances (Fig. S2). The extremely large difference between the highest and lowest REE abundances in the equilibrium melts (Fig. 5) could not result from simple fractional crystallization in a single magma (LMO), and it must be related to mixing of different materials. At least three different end-members would be required to produce such large REE variations in melt equilibrated with anorthositic plagioclase (Fig. 5; see also Figs. S4 and S5).

One end-member that controls the Eu is probably related to the primordial anorthosite (PAN) directly crystallized from the LMO. Therefore, this end-member would probably be melt in equilibrium with the PAN in the mixing models (Fig. 5). The other two end-members are inferred to have opposite REE patterns and different absolute REE compositions according to the variations of trace elements (Fig. 5). They could be KREEP and melts derived from the early LMO mantle cumulates. As the LMO crystallization continued, the REE abundances of the residual melt increased with decreasing Mg#. The last dregs of melt residue, urKREEP, were extremely rich in Fe and incompatible trace elements, including REE (Warren, 1985; 1989). The widespread distribution and high REE abundances (Fig. 5; see also Figs. S4 and S5; Warren, 1985) indicate that urKREEP melt could be the second end-member. Some equilibrium melts are more HREE-enriched than others (Fig. S2). The HREE-rich melts have not been observed in the LMO melt residue (Snyder et al., 1992). However, the mantle cumulates that crystallized from the LMO could be rich in HREE (Snyder et al., 1992). Therefore, melts derived from the LMO cumulates could be the third end-member. This end-member could also have high Mg# (Figs. 2a, 4g, and 4h). In summary, three melt end-members in equilibrium with lunar anorthosites have been identified (Figs. 4 and 5; see also Figs. S4 and S5).

The boundaries of the compositional field of REE in melt equilibrated with anorthositic plagioclase may be quantified using mixing models (Langmuir et al., 1978) with different end-members (Fig. 5; see also Figs. S4 and S5). To simplify the modeling procedure, three melt end-members are used: m-PAN, m-KREEP, and m-Mantle (Fig. 6; Table 3), representing melt in equilibrium with the primordial anorthosite, urKREEP melt, and melt derived from the LMO mantle cumulates, respectively. The mixing lines established by the three melt end-members envelop most available data of equilibrium melts (Fig. 5; see also Figs. S4 and S5). Note that these three end-members are the extremes, and the role of crystal fractionation of the LMO (i.e., different chemical compositions of PAN, as well as those of mantle cumulates) is not considered in our mixing model. Owing to the complexities of magma fractional crystallization and mantle partial melting, the real melt end-members for an individual lunar anorthosite may lie inside the compositional field outlined by the three end-members, m-PAN, m-KREEP, and m-Mantle. The melt compositions within the fields could be produced through mixing of available end-members (Fig. 5; see also Figs. S4 and S5). Therefore, our mixing

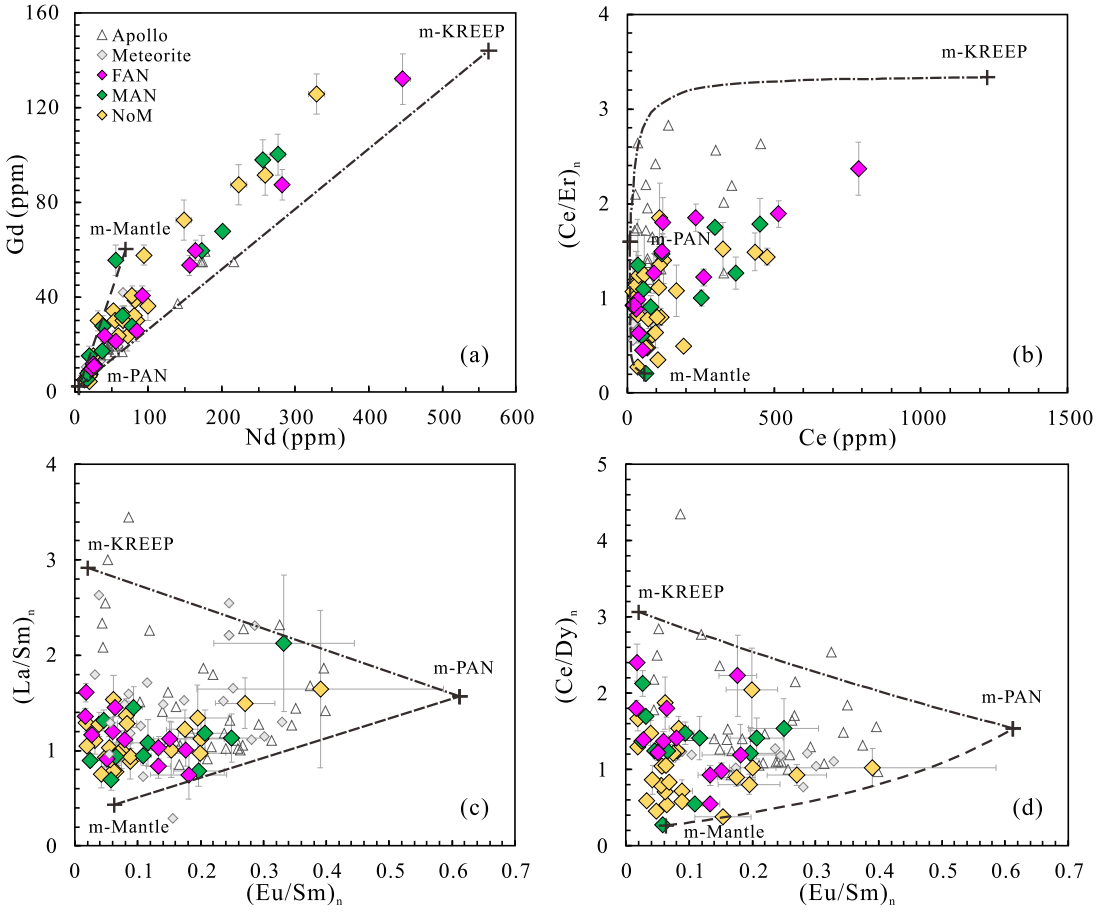

Fig. 5. Covariation of REE in melt equilibrated with anorthositic plagioclase. The dashed lines represent mixing models between different end-members (m-PAN, m-Mantle, and m-KREEP). Subscript "n" denotes chondrite normalized. All mixing plots are shown in the supplementary material (Figs. S4 and S5).

model is illustrative of the different chemical components recorded by the lunar anorthosite compositions. However, the mixing mechanism is not a simple mixing of three different magmas, but infiltration and metasomatization of the primordial crust by the two melt end-members of m-KREEP and m-Mantle (see the discussion below).

Among the three melt end-members, m-PAN has the lowest REE abundances, and it has slightly smaller negative Eu anomaly than those of melt in equilibrium with Apollo anorthositic plagioclase (Fig. 6; Table 3). This difference suggests that the primordial anorthosite in equilibrium with the end-member m-PAN crystallized earlier among all available anorthosites that may have directly crystallized from the LMO. The end-member m-KREEP has the highest REE abundances (Fig. 6). The REE patterns of m-KREEP and high-K KREEP are nearly parallel to each other, with m-KREEP being slightly richer in LREE and with a more negative Eu/Eu* than high-K KREEP (Fig. 6; Warren, 1989). This is consistent with the proposed difference between urKREEP and high-K KREEP (Neal and Taylor, 1989). Furthermore, m-KREEP has a REE pattern similar to that of the LREE-enriched über-KREEP liquid proposed by Cronberger and Neal (2018; 2019), both of which have much higher REE abundances than the high-K KREEP defined by Warren (1989). Furthermore, this end-member would be rich in Fe (Snyder et al., 1992) and thus decrease the Mg# of mafic minerals in the anorthosites. In summary, the end-member m-KREEP in this model is considered as urKREEP. The end-member m-Mantle is rich in HREE (Fig. 6), consistent with its origin as partial melts from mantle cumulates directly derived from the LMO (Snyder et al., 1992). This mantle end-member could have also increased the Mg# of anorthosite (Figs. 2a, 4g and 4h). Therefore, the melts in equilibrium with anorthositic plagioclases could be geochemically explained by mixing of the three melt end-members.

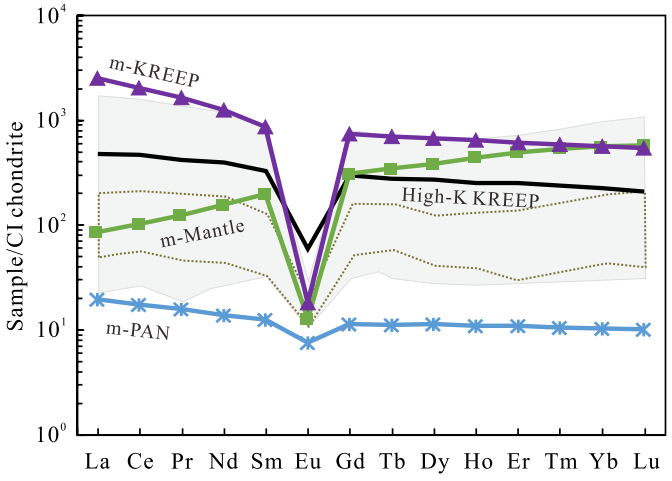

Fig. 6. CI-chondrite normalized REE patterns of three end-members. CI chondrite compositions are from Anders and Grevesse (1989). The field outlined by dashed lines represents the range of melt in equilibrium with plagioclase in Apollo FANs (Floss et al., 1998; Papike et al., 1997). The shaded area represents the range of melt in equilibrium with plagioclase in meteoritic anorthosites (Russell et al., 2014; Pernet-Fisher et al., 2017). The black line represents high-K KREEP composition (Warren, 1989). The blue line represents the end-member m-PAN. The green line represents the end-member m-Mantle. The purple line represents the end-member m-KREEP. (For interpretation of the colors in the figure(s), the reader is referred to the web version of this article.)

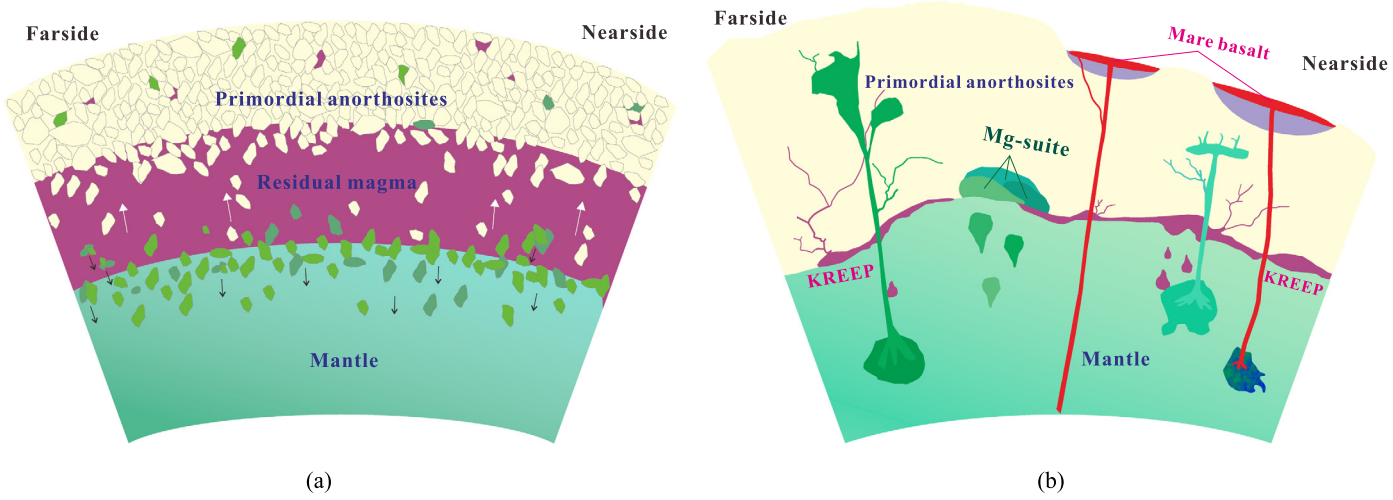

Fig. 7. Schematic diagram of the formation of lunar anorthosites. (a) Plagioclase crystallizes in the LMO and then floats to form the primordial anorthositic crust, which represents source region of end-member m-PAN. Denser minerals sink to form the mantle, which could be the source region of end-member m-Mantle. As the LMO crystallization continues, the residual melt becomes richer in incompatible trace elements and forms urKREEP, resulting in end-member m-KREEP. (b) The upwelling KREEP melt (m-KREEP) and partial melts derived from the mantle (m-Mantle) percolate through and metasomatize the primordial anorthositic crust (m-PAN). Some intruded melts could melt portions of the crust to form Mg-suite rocks.

4.4. Formation of lunar anorthosites

It is generally accepted that the primordial lunar feldspathic crust directly crystallized from the LMO (Fig. 7a; e.g. Snyder et al., 1992). This primordial crust could have contained anorthosite in equilibrium with the end-member m-PAN (Fig. 5), as well as some FANs crystallized directly from the LMO. This crust could not have appeared as melt during mixing but rather as solid crust (Fig. 7b). The formation of the primordial crust could be very rapid, likely within the first 10 Myr after the formation of the Moon (Elkins-Tanton et al., 2011). This mixing process could then have occurred by means of metasomatism, and the REE compositions in lunar anorthosites, as well as the large range of Mg# in mafic minerals (Fig. 2a), could have resulted from metasomatism of primordial feldspathic crust by the two melt end-members m-KREEP and m-Mantle. Note that impact process could also mix different components and alter the REE distribution patterns in plagioclase (Cahill et al., 2004; Pernet-Fisher et al., 2017). However, impact melting could produce plagioclase with chemical zonation (e.g., Hui et al., 2011), which is not consistent with the geochemically homogeneous plagioclase grain within each anorthosite investigated in this study. Furthermore, impact process on the Moon has lasted for a very long time (Stöffler et al., 2006), much longer than the formation period of highlands rocks, including anorthosite (Borg et al., 2015). If impact processes were the main mechanism to mix different end-members in the manner described here to form lunar anorthosites, the chronometers would be reset and there would be anorthosites with ages much younger than those already recorded. This suggestion is not consistent with our observation that anorthosites are older than 4.2 Ga (Borg et al., 2015). Finally, many FANs formed at depth of 10–20 km (McCallum and O'Brien, 1996), where crystallization unlikely resulted from impact process. Therefore, the impact process cannot be the main mixing mechanism.

The high REE abundances in anorthositic plagioclase could have been produced by crustal metasomatism (e.g., Neal and Taylor, 1989; 1991) of the melt end-member m-KREEP (Fig. 7b). The continuous crystallization of the LMO residual melt underneath the primordial anorthositic crust leads to progressively enrichment in incompatible trace elements and Fe (Snyder et al., 1992). The residual melt rich in KREEP composition may have infiltrated into and metasomatized the primordial crust. The metasomatism of primordial crust (represented by m-PAN) by m-KREEP could enrich REE abundances in anorthositic plagioclase and decrease the Mg# of mafic minerals. It has been suggested that urKREEP could have undergone an unmixing process to produce two immiscible melts, a granitic K-rich melt and a ferrobasaltic REEP-rich melt (Neal and Taylor, 1989; 1991). The low viscous ferrobasaltic REEP-rich melt could also percolate and metasomatize the primordial lunar crust (Neal and Taylor, 1989; 1991). Either way, the primordial anorthosites could have been metasomatized by the melt containing the KREEP component and produced REE-rich plagioclase and Fe-rich mafic minerals.

The third end-member of lunar anorthosites is LREE depleted (Fig. 6), which would be the REE pattern of the early Mg-rich LMO cumulates (Snyder et al., 1992). In order to generate a LREE-depleted melt from these early LMO cumulates, a large degree of partial melting would be required. This could be achieved through decompression melting during cumulate overturn. Therefore, the MAN samples may record this overturn event. The LREE-depleted signature of parent melts of some mare basalts (e.g., Neal and Taylor, 1992; Hallis et al., 2014) suggests that partial melting of the lunar mantle could produce the end-member m-Mantle. The upwelling melts of m-Mantle could have percolated into and metasomatized the lunar anorthositic crust (Fig. 7b). This metasomatism could have resulted in HREE enrichment in anorthositic plagioclase and formation of mafic minerals with high Mg#. The partial melting of lunar mantle could have been caused by decompression during an early mantle overturn before the one that generated mare basalts. This proposal is consistent with the pre-mare volcanism observed in the lunar highlands and potential the cryptomare (e.g., Taylor et al., 1983; Hui et al., 2013; Whitten and Head, 2015).

During metasomatism, both Mg- and Fe-rich mafic minerals could have formed locally in the lunar anorthositic crust, consistent with the large Mg# variation in anorthosites (Fig. 2a). Plagioclases and their coexisting mafic minerals in the anorthosite samples may not have reached equilibrium. Moreover, percolation of KREEP-rich melts could have enriched REE abundances in anorthositic plagioclases to different degrees. Therefore, the metasomatic temperatures in lunar anorthositic crust were below the melting temperature of anorthositic plagioclase. The metasomatism of lunar anorthosite in crust is also consistent with the low cooling rates (10–37 °C/Myr) estimated for FANs 60016, 60025, and 67075 (McCallum and O'Brien, 1996; Marks et al., 2019).

Alternatively, the end-member metasomatic melts, m-KREEP and m-Mantle, could have intruded into the anorthositic crust. Instead of metasomatism, the m-Mantle melts may have melted plagioclase and formed different highlands lithologies such as the Mg-suite that evolved to alkali-suite compositions (Fig. 7b; Shervais and McGee, 1998). This melting scenario is consistent with the proposal that the Mg-suite rocks were produced by interactions of mantle-derived melts, KREEP-rich melts, and primordial anorthositic crust (Shearer et al., 2015). Thus, owing to different mixing proportions of end-members and crystal fractionation in magmas, the plutonic HMS lithologies also exhibit a wide range of compositions, including dunite, troctolite, norite, and gabbronorite (Shearer et al., 2015).

4.5. Implications for ages of highlands lithologies

The Sm-Nd isotope ages of lunar anorthosites vary from 4.29 to 4.57 Ga, similar to those determined for Mg-suite rocks, which range from 4.16 Ga to 4.55 Ga (Borg et al., 2015, and references therein). Our model is consistent with the age similarity between Mg-suite rocks and anorthosites. The primordial lunar crust could have formed very early through fractional crystallization of the LMO (Elkins-Tanton et al., 2011; Barboni et al., 2017). KREEP melts derived from the last dregs of the LMO melt residue and melts produced by extensive cumulate melting during overturn of the early cumulate mantle could have intruded into the crust. Some portions of the primordial crust may have been metasomatized to form the lunar anorthosites (Fig. 7). Alternatively, some portions of the primordial crust affected by the partial melts from mantle could have even been melted, thereby forming the parent magmas of Mg-suite rocks (Fig. 7). The metasomatism and melting could have occurred at the same time after formation of the primordial crust. Therefore, the ages of the two different rock suites would overlap. However, zircon may have still recorded the crystallization age of the primordial crust, which is the oldest (Barboni et al., 2017).

Limited data indicate that both lunar anorthosites and Mg-suite rocks have a wide range of initial ε_{Nd} values, varying from positive to negative (Fig. S6; Borg et al., 2015). This wide range suggests that lunar anorthosites could have multiple source regions, including mantle, primary crust, and urKREEP. The radiometric ages and hence the initial ε_{Nd} values of lunar anorthosites could have been reset by metasomatism, consistent with REE patterns in anorthositic plagioclase (Fig. 5). The similar initial ε_{Nd} values in FAN-MAN anorthosites and Mg-suite rocks (Fig. S6) are consistent with them being derived from similar source regions (i.e., end-members). Finally, the impact process cannot explain the similarities both in age and initial ε_{Nd} values between the magnesian and ferroan anorthosites and Mg-suite rocks.

5. Concluding remarks

We report new *in situ* major and trace element compositions of plagioclases in ten lunar feldspathic meteorites. The Mg# of mafic minerals in anorthositic clasts range from 49.9 to 80.1, and their plagioclase An vary from 95.3 to 98.4. The differences in REE abundances in anorthositic plagioclase are as large as about forty-fold, in line with the reported in previous studies (e.g., Russell et al., 2014). This large difference is not consistent with simple fractional crystallization of a single magma. Rather, the REE distributions in anorthositic plagioclase from both Apollo and lunar meteorite samples may be best explained by silicate melt metasomatism in the primordial lunar crust directly derived from the LMO. The metasomatic melts include KREEP melts that originated from the last dregs of the LMO residue (urKREEP), and large degree decompression melts of the early LMO cumulates due to overturn of the mantle cumulate pile. This metasomatism can also explain the large ranges observed for age and initial ε_{Nd} values in lunar anorthosites. In addition, the Mg-suite rocks and the FAN-MAN anorthosites could have similar source regions (i.e., end-members), consistent with the observed similarities in age and initial ε_{Nd} values.

Declaration of competing interest

The authors declare that they have no known competing financial interests or personal relationships that could have appeared to influence the work reported in this paper.

Acknowledgements

This research is supported by NSFC grants (41573055 and 41590623). We thank editor Fred Moynier for handling our manuscript and an anonymous reviewer for critical and thorough reviews.

Appendix A. Supplementary material

Supplementary material related to this article can be found online at https://doi.org/10.1016/j.epsl.2020.116138.

References

Albarède, F., 1995. Introduction to Geochemical Modeling. Cambridge University Press, Cambridge, England.
Anders, E., Grevesse, N., 1989. Abundances of the elements: meteoritic and solar. Geochim. Cosmochim. Acta 53, 197–214.
Barboni, M., Boehnke, P., Keller, B., Kohl, I.E., Schoene, B., Young, E.D., McKeegan, K.D., 2017. Early formation of the Moon 4.51 billion years ago. Sci. Adv. 3, e1602365.
Borg, L.E., Connelly, J.N., Boyet, M., Carlson, R.W., 2011. Chronological evidence that the Moon is either young or did not have a global magma ocean. Nature 477, 70–72.
Borg, L.E., Gaffney, A.M., Kruijer, T.S., Marks, N.A., Sio, C.K., Wimpenny, J., 2019. Isotopic evidence for a young lunar magma ocean. Earth Planet. Sci. Lett. 523, 115706.
Borg, L.E., Gaffney, A.M., Shearer, C.K., 2015. A review of lunar chronology revealing a preponderance of 4.34–4.37 Ga ages. Meteorit. Planet. Sci. 50, 715–732.
Cahill, J.T., Floss, C., Anand, M., Taylor, L.A., Nazarov, M.A., Cohen, B.A., 2004. Petrogenesis of lunar highlands meteorites: Dhofar 025, Dhofar 081, Dar al Gani 262, and Dar al Gani 400. Meteorit. Planet. Sci. 39, 503–530.
Canup, R.M., Asphaug, E., 2001. Origin of the Moon in a giant impact near the end of the Earth's formation. Nature 412, 708–712.
Cronberger, K., Neal, C.R., 2018. Origin(s) and evolution of KREEP basalts. Lunar Planet. Sci. Conf. 49, 1305.
Cronberger, K., Neal, C.R., 2019. KREEP Basalt 15382: not as pristine as originally thought. Lunar Planet. Sci. Conf. 50, 2444.
Dixon, J.R., Papike, J.J., 1975. Petrology of anorthosites from the Descartes region of the moon: Apollo 16. In: Proc. Lunar Planet. Sci. Conf. 6th, pp. 263–291.
Elardo, S.M., Draper, D.S., Shearer, C.K., 2011. Lunar magma ocean crystallization revisited bulk composition, early cumulate mineralogy, and the source regions of the highlands Mg-suite. Geochim. Cosmochim. Acta 75, 3024–3045.
Elkins-Tanton, L.T., 2012. Magma oceans in the inner solar system. Annu. Rev. Earth Planet. Sci. 40, 113–139.
Elkins-Tanton, L.T., Burgess, S., Yin, Q.Z., 2011. The lunar magma ocean: reconciling the solidification process with lunar petrology and geochronology. Earth Planet. Sci. Lett. 304, 326–336.
Evans, H.T., Huebner, J.S., Konnert, J.A., 1978. The crystal structure and thermal history of orthopyroxene from lunar anorthosite 15415. Earth Planet. Sci. Lett. 37, 476–484.
Floss, C., James, O.B., McGee, J.J., Crozaz, G., 1998. Lunar ferroan anorthosite petrogenesis: clues from trace element distributions in FAN subgroups. Geochim. Cosmochim. Acta 62, 1255–1283.
Goodrich, C.A., Taylor, G.J., Keil, K., Boynton, W.V., Hill, D.H., 1984. Petrology and chemistry of hyperferroan anorthosites and other clasts from lunar meteorite ALHA 81005. J. Geophys. Res. 89, 87–94.
Gross, J., Treiman, A.H., Mercer, C.N., 2014. Lunar feldspathic meteorites: constraints on the geology of the lunar highlands, and the origin of the lunar crust. Earth Planet. Sci. Lett. 388, 318–328.
Hallis, L.J., Anand, M., Strekopytov, S., 2014. Trace-element modelling of mare basalt parental melts: implications for a heterogeneous lunar mantle. Geochim. Cosmochim. Acta 134, 289–316.

Hess, P.C., Parmentier, E.M., 1995. A model for the thermal and chemical evolution of the Moon's interior: implications for the onset of mare volcanism. Earth Planet. Sci. Lett. 134, 501–514.
Hui, H., Neal, C.R., Shih, C.-Y., Nyquist, L.E., 2013. Petrogenetic association of the oldest lunar basalts: combined Rb-Sr isotopic and trace element constraints. Earth Planet. Sci. Lett. 373, 150–159.
Hui, H., Oshrin, J.G., Neal, C.R., 2011. Investigation into the petrogenesis of Apollo 14 high-Al basaltic melts through crystal stratigraphy of plagioclase. Geochim. Cosmochim. Acta 75, 6439–6460.
James, O.B., Floss, C., McGee, J.J., 2002. Rare earth element variations resulting from inversion of pigeonite and subsolidus reequilibration in lunar ferroan anorthosites. Geochim. Cosmochim. Acta 66, 1269–1284.
James, O.B., Lindstrom, M.M., Flohr, M.K., 1989. Ferroan anorthosite from lunar breccia 64435: implications for the origin and history of lunar ferroan anorthosites. In: Proc. Lunar Planet. Sci. Conf. 19th, pp. 219–243.
Jolliff, B.L., Haskin, L.A., 1995. Cogenetic rock fragments from a lunar soil: evidence of a ferroan noritic-anorthosite pluton on the Moon. Geochim. Cosmochim. Acta 59, 2345–2374.
Korotev, R.L., 2005. Lunar geochemistry as told by lunar meteorites. Chem. Erde 65, 297–346.
Langmuir, C.H., Vocke, R.D., Hanson, G.N., Hart, S.R., 1978. A general mixing equation with applications to Icelandic basalts. Earth Planet. Sci. Lett. 37, 380–392.
Lindstrom, M.M., Marvin, U.B., Mittlefehldt, D.W., 1989. Apollo 15 Mg- and Fe-norites: a redefinition of the Mg-suite differentiation trend. In: Proc. Lunar Planet. Sci. Conf. 19th, pp. 245–254.
Liu, Y., Hu, Z., Gao, S., Günther, D., Xu, J., Gao, C., Chen, H., 2008. *In situ* analysis of major and trace elements of anhydrous minerals by LA-ICP-MS without applying an internal standard. Chem. Geol. 257, 34–43.
Longhi, J., 1982. Effects of fractional crystallization and cumulus processes on mineral composition trends of some lunar and terrestrial rock series. J. Geophys. Res. 87, A54–A64.
Longhi, J., 2003. A new view of lunar ferroan anorthosites: postmagma ocean petrogenesis. J. Geophys. Res. 108, 5083. https://doi.org/10.1029/2002JE001941.
Marks, N.E., Borg, L.E., Shearer, C.K., Cassata, W.S., 2019. Geochronology of an Apollo 16 clast provides evidence for a basin-forming impact 4.3 billion years ago. J. Geophys. Res., Planets 124, 2465–2481.
McCallum, I.S., O'Brien, H.E., 1996. Stratigraphy of the lunar highland crust: depths of burial of lunar samples from cooling-rate studies. Am. Mineral. 81, 1166–1175.
McGee, J.J., 1993. Lunar ferroan anorthosites: mineralogy, compositional variations, and petrogenesis. J. Geophys. Res. 98, 9089–9105.
Mercer, C.N., Treiman, A.H., Joy, K., 2013. New lunar meteorite Northwest Africa 2996: a window into farside highlands lithologies and petrogenesis. Meteorit. Planet. Sci. 48, 289–315.
Namur, O., Charlier, B., Pirard, C., Hermann, J., Liégeois, J.P., Vander Auwera, J., 2011. Anorthosite formation by plagioclase flotation in ferrobasalt and implications for the lunar crust. Geochim. Cosmochim. Acta 75, 4998–5018.
Neal, C.R., Taylor, L.A., 1989. Metasomatic products of the lunar magma ocean: the role of KREEP dissemination. Geochim. Cosmochim. Acta 53, 529–541.
Neal, C.R., Taylor, L.A., 1991. Evidence for metasomatism of the lunar highlands and the origin of whitlockite. Geochim. Cosmochim. Acta 55, 2965–2980.
Neal, C.R., Taylor, L.A., 1992. Petrogenesis of mare basalts: a record of lunar volcanism. Geochim. Cosmochim. Acta 56, 2177–2211.
Nekvasil, H., Lindsley, D.H., DiFrancesco, N., Catalano, T., Coraor, A.E., Charlier, B., 2015. Uncommon behavior of plagioclase and the ancient lunar crust. Geophys. Res. Lett. 42, 10573–10579.
Ohtake, M., Takeda, H., Matsunaga, T., Yokota, Y., Haruyama, J., Morota, T., Yamamoto, S., Ogawa, Y., Hiroi, T., Karouji, Y., Saiki, K., Lucey, P.G., 2012. Asymmetric crustal growth on the Moon indicated by primitive farside highland materials. Nat. Geosci. 5, 384–388.
Palme, H., Spettel, B., Wänke, H., Bischoff, A., Stöffler, D., 1984. Early differentiation of the Moon: evidence from trace elements in plagioclase. J. Geophys. Res. 89, C3–C15.
Papike, J.J., Fowler, G.W., Shearer, C.K., 1997. Evolution of the lunar crust: SIMS study of plagioclase from ferroan anorthosites. Geochim. Cosmochim. Acta 61, 2343–2350.
Papike, J.J., Fowler, G.W., Shearer, C.K., Layne, G.D., 1996. Ion microprobe investigation of plagioclase and orthopyroxene from lunar Mg-suite norites: implications for calculating parental melt REE concentrations and for assessing postcrystallization REE redistribution. Geochim. Cosmochim. Acta 60, 3967–3978.
Pernet-Fisher, J.F., Joy, K.H., Martin, D.J.P., Hanna, K.D., 2017. Assessing the shock state of the lunar highlands: implications for the petrogenesis and chronology of crustal anorthosites. Sci. Rep. 7, 5888.
Russell, S.S., Joy, K.H., Jeffries, T.E., Consolmagno, G.J., Kearsley, A., 2014. Heterogeneity in lunar anorthosite meteorites: implications for the lunar magma ocean model. Philos. Trans. R. Soc. A 372, 20130241.
Shearer, C.K., et al., 2006. Thermal and magmatic evolution of the Moon. Rev. Mineral. Geochem. 60, 365–518.
Shearer, C.K., Elardo, S.M., Petro, N.E., Borg, L.E., McCubbin, F.M., 2015. Origin of the lunar highlands Mg-suite: an integrated petrology, geochemistry, chronology, and remote sensing perspective. Am. Mineral. 100, 294–325.
Shervais, J.W., McGee, J.J., 1998. Ion and electron microprobe study of Mg suite troctolites, norite, and anorthosites from Apollo 14: evidence for urKREEP assimilation during petrogenesis of Apollo 14 Mg-suite rocks. Geochim. Cosmochim. Acta 62, 3009–3023.
Snyder, G.A., Taylor, L.A., Neal, C.R., 1992. A chemical model for generating the sources of mare basalts: combined equilibrium and fractional crystallization of the lunar magmasphere. Geochim. Cosmochim. Acta 56, 3809–3823.
Steele, I.M., Hutcheon, I.D., Smith, J.V., 1980. Ion microprobe analysis and petrogenetic interpretations of Li, Mg, Ti, K, Sr, Ba in lunar plagioclase. In: Proc. Lunar Planet. Sci. Conf. 11th, pp. 571–590.
Stöffler, D., Ryder, G., Ivanov, B.A., Artemieva, N.A., Cintala, M.J., Grieve, R.A., 2006. Cratering history and lunar chronology. Rev. Mineral. Geochem. 60, 519–596.
Sun, C., Graff, M., Liang, Y., 2017. Trace element partitioning between plagioclase and silicate melt: the importance of temperature and plagioclase composition, with implications for terrestrial and lunar magmatism. Geochim. Cosmochim. Acta 206, 273–295.
Takeda, H., Yamaguchi, A., Bogard, D.D., Karouji, Y., Ebihara, M., Ohtake, M., Saiki, K., Arai, T., 2006. Magnesian anorthosites and a deep crustal rock from the farside crust of the Moon. Earth Planet. Sci. Lett. 247, 171–184.
Taylor, L.A., Shervais, J.W., Hunter, R.H., Shih, C.-Y., Bansal, B.M., Wooden, J., Nyquist, L.E., Laul, L.C., 1983. Pre-4.2 AE mare-basalt volcanism in the lunar highlands. Earth Planet. Sci. Lett. 66, 33–47.
Togashi, S., Kita, N.T., Tomiya, A., Morishita, Y., 2017. Magmatic evolution of lunar highland rocks estimated from trace elements in plagioclase: a new bulk silicate Moon model with sub-chondritic Ti/Ba, Sr/Ba, and Sr/Al ratios. Geochim. Cosmochim. Acta 210, 152–183.
Warren, P.H., 1985. The magma ocean concept and lunar evolution. Annu. Rev. Earth Planet. Sci. 13, 201–240.
Warren, P.H., 1989. KREEP: major-element diversity, trace-element uniformity (almost). In: Taylor, G.J., Warren, P.H. (Eds.), Workshop on Moon in Transition: Apollo 14, KREEP, and Evolved Lunar Rocks, pp. 149–153. LPI Tech. Rpt. 89-03. Lunar and Planetary Institute, Houston.
Warren, P.H., 1993. A concise compilation of petrologic information on possibly pristine nonmare Moon rocks. Am. Mineral. 78, 360–376.
Whitten, J.L., Head, J.W., 2015. Lunar cryptomaria: physical characteristics, distribution, and implications for ancient volcanism. Icarus 247, 150–171.